Parallel-Processing Astrophysical Image-Analysis Tools

Kenneth John Mighell

National Optical Astronomy Observatory

NOAO

Outline

- Spitzer Space Telescope's Infrared Array Camera
- A Systematic Centroid Error
- Porting CRBLASTER to the Maestro Processor

Spitzer Space Telescope's Infrared Array Camera

Infrared Array Camera

Spitzer Space Telescope

ID	RA_HMS	DEC_DMS	EXPTIME	DATE_OBS	DS_IDENT
1	17h06m11.6s	+73d40m11s	0.4	2003-10-08T11:55:51.356	ads/sa.spitzer#0006875392
2	17h06m11.1s	+73d40m11s	0.4	2003-10-08T12:08:56.748	ads/sa.spitzer#0006876672
3	17h06m10.8s	+73d40m10s	0.4	2003-10-08T12:22:01.538	ads/sa.spitzer#0006876928
4	17h06m10.6s	+73d40m09s	0.4	2003-10-08T12:35:06.524	ads/sa.spitzer#0006877184
5	17h06m11.3s	+73d40m12s	0.4	2003-10-08T12:48:11.510	ads/sa.spitzer#0006877440
6	17h06m10.9s	+73d40m12s	0.4	2003-10-08T13:01:16.496	ads/sa.spitzer#0006877696
7	17h06m10.5s	+73d40m11s	0.4	2003-10-08T13:14:21.489	ads/sa.spitzer#0006877952
8	17h06m10.2s	+73d40m11s	0.4	2003-10-08T13:27:26.471	ads/sa.spitzer#0006878208
9	17h06m11.0s	+73d40m14s	0.4	2003-10-08T13:40:31.472	ads/sa.spitzer#0006878464
10	17h06m10.7s	+73d40m13s	0.4	2003-10-08T13:53:36.446	ads/sa.spitzer#0006878720
11	17h06m10.5s	+73d40m13s	0.4	2003-10-08T14:06:41.436	ads/sa.spitzer#0006878976
12	17h06m10.0s	+73d40m12s	0.4	2003-10-08T14:19:46.422	ads/sa.spitzer#0006879232
13	17h06m11.0s	+73d40m15s	0.4	2003-10-08T14:32:51.423	ads/sa.spitzer#0006879488
14	17h06m10.5s	+73d40m15s	0.4	2003-10-08T15:06:39.788	ads/sa.spitzer#0006879744
15	17h06m10.3s	+73d40m14s	0.4	2003-10-08T15:19:44.785	ads/sa.spitzer#0006880000
16	17h06m10.0s	+73d40m13s	0.4	2003-10-08T15:32:49.763	ads/sa.spitzer#0006880256

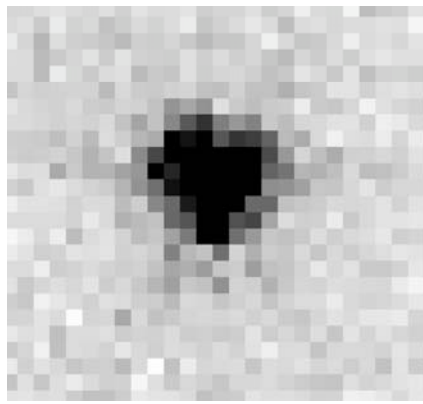

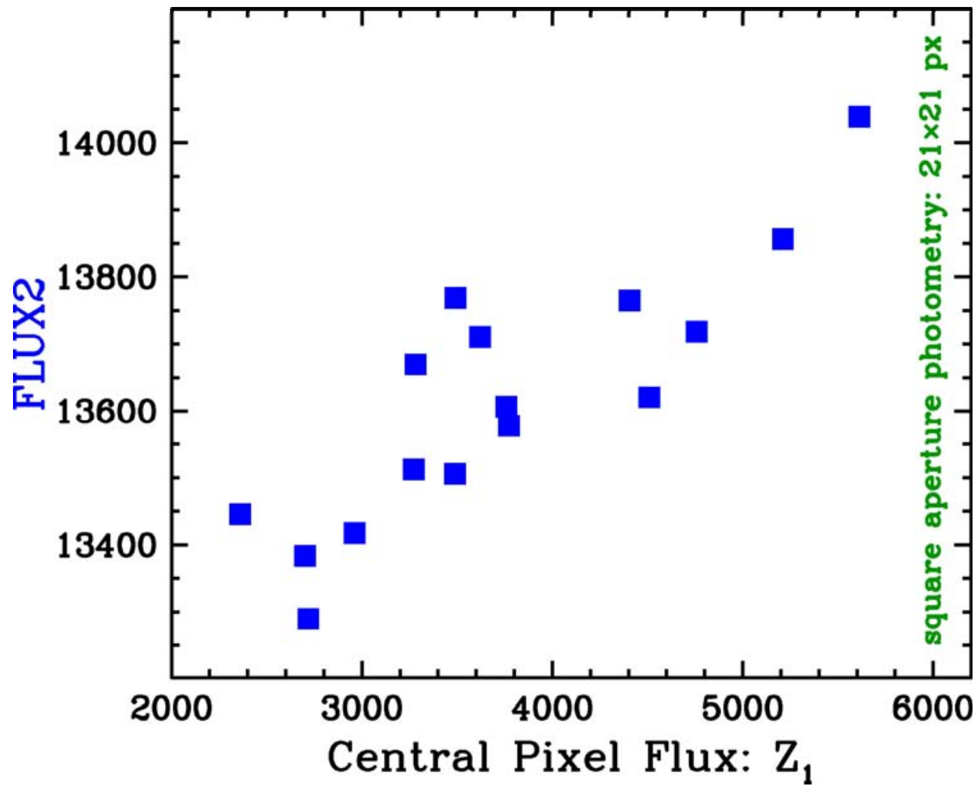

Not all of the variation is random!

Stars centered in the middle of a pixel have more flux than those that are centered on a pixel corner.

IRAC Ch1 PSF (5x5 theoretical)

linear stretch

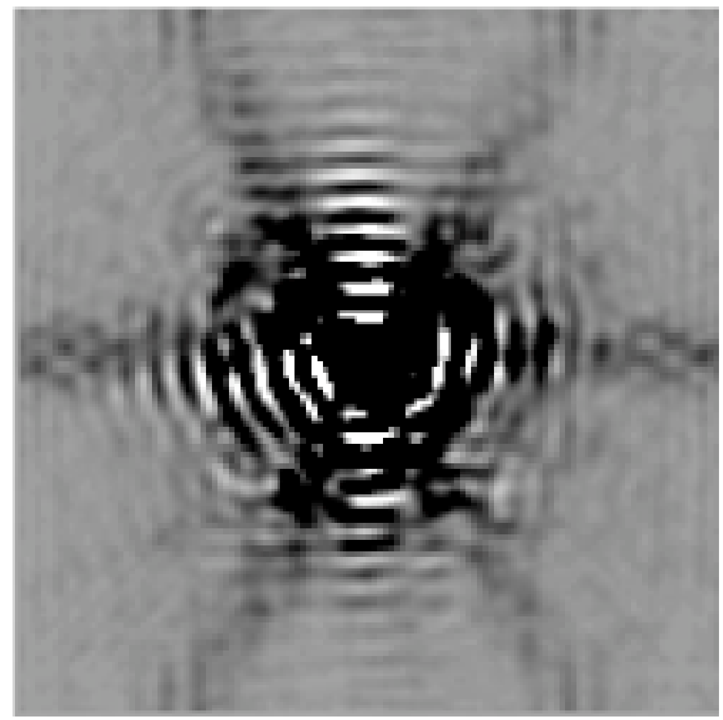

logarithmic stretch

Source: Bill Hoffmann
(U. of Arizona, IRAC team member)

Relative Intrapixel QE Variation of IRAC Ch1

$$\text{intrapix} = \begin{pmatrix} 0.813 & 0.875 & 0.875 & 0.875 & 0.813 \\ 0.875 & 1.000 & 1.000 & 1.000 & 0.875 \\ 0.875 & 1.000 & 1.000 & 1.000 & 0.875 \\ 0.875 & 1.000 & 1.000 & 1.000 & 0.875 \\ 0.813 & 0.875 & 0.875 & 0.875 & 0.813 \end{pmatrix}$$

Source: Bill Hoffmann
(U. of Arizona, IRAC team member)

IRAC Data Handbook

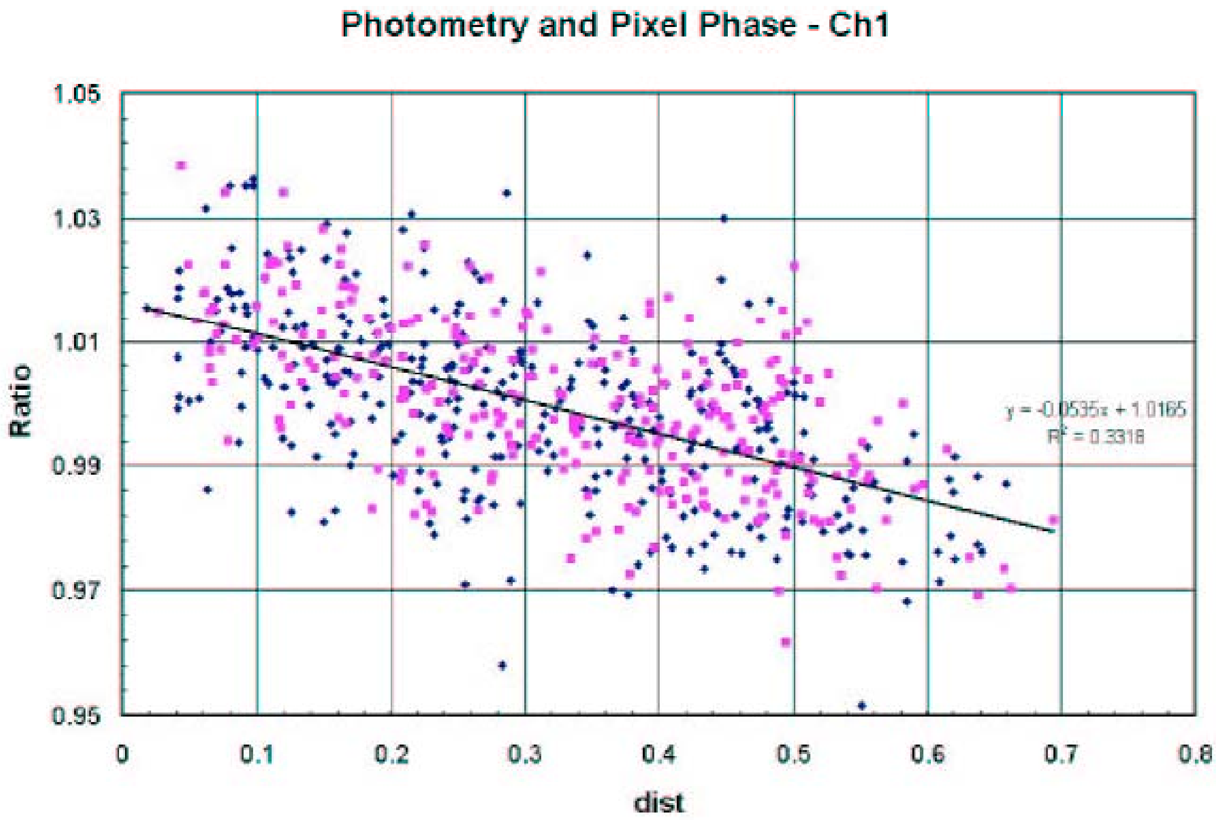

Figure 5.1: Dependence of point source photometry on the distance of the centroid of a point source from the nearest pixel center in channel 1. The ratio on the vertical axis is the measured flux density to the mean value for the star, and the quantity on the horizontal axis is the fractional distance of the centroid from the nearest pixel center.

Point Response Function ▼ ▼ Point Spread Function

$$\Psi \equiv \phi * \Lambda$$

▲ **D**etector **R**esponse **F**unction

$$\Psi_i(x_i, y_i) \equiv \int_{x_i-0.5}^{x_i+0.5} \int_{y_i-0.5}^{y_i+0.5} \phi(x, y)\, dx\, dy \quad \text{(for an ideal DRF)}$$

$$\mathrm{V} \equiv \int_{-\infty}^{\infty} \int_{-\infty}^{\infty} \Psi\, dx\, dy \lesssim 1$$

Volume ▲

$$\text{sharpness} \equiv \int_{-\infty}^{\infty} \int_{-\infty}^{\infty} \left(\frac{\Psi}{\mathrm{V}}\right)^2 dx\, dy$$

▲ normalized PRF

$$\beta \equiv \left[\iint_{-\infty}^{\infty} \Psi^2\, dx\, dy\right]^{-1} = \frac{1}{\mathrm{V}^2\, \text{sharpness}}$$

Effective Background Area ▲

$$\mathcal{L} \equiv \sqrt{\frac{\beta\, \mathrm{V}^2}{4\pi}} = \frac{1}{\sqrt{4\pi\, \text{sharpness}}}$$

Critical-Sampling Scale Length ▲

background level ▼ ▼ volume of Point Response Function

$$m_i \equiv \mathcal{B} + \mathcal{E}\mathrm{V}\tilde{\Psi}_i$$

pixel value ▲ ▲ normalized PRF
stellar intensity [electrons] ▲

$$\tilde{\Psi}_i(x_i, y_i) \equiv \int_{x_i-0.5}^{x_i+0.5} \int_{y_i-0.5}^{y_i+0.5} \phi(x,y)\, dx\, dy \quad (\text{ideal DRF: } \mathrm{V} \equiv 1)$$

▲ Point Spread Function

$$\mathsf{S/N} \equiv \frac{\mathcal{E}}{\sigma_{\mathcal{E}}} \approx \frac{\mathcal{E}}{\sqrt{\frac{\mathcal{E}}{\mathrm{V}} + \beta\left(1 + \sqrt{\beta/N}\right)^2 \left[\mathcal{B} + \sigma^2_{\mathrm{RON}}\right]}}$$

signal-to-noise ratio ▲

▲ readout noise

▲ aperture size [pixels]

$$\Delta\mathsf{mag} \approx \frac{1.0857}{\mathsf{S/N}}$$

▲ Effective Background Area

▼Critical-Sampling Scale Length

$$\sigma_{\mathcal{X}} \approx \sqrt{\frac{\mathcal{L}^2}{\mathcal{E}\mathrm{V}}\left[1 + 8\pi\left(\mathcal{B} + \sigma^2_{\mathrm{RON}}\right)\frac{\mathcal{L}^2}{\mathcal{E}\mathrm{V}}\right]}$$

$$\sigma_{\mathcal{Y}} = \sigma_{\mathcal{X}}$$

Mon. Not. R. Astron. Soc. **361**, 861–878 (2005) doi:10.1111/j.1365-2966.2005.09208.x

Stellar photometry and astrometry with discrete point spread functions

Kenneth J. Mighell*
National Optical Astronomy Observatory, 950 North Cherry Avenue, Tucson, AZ 85719, USA

Lost flux can be recovered!

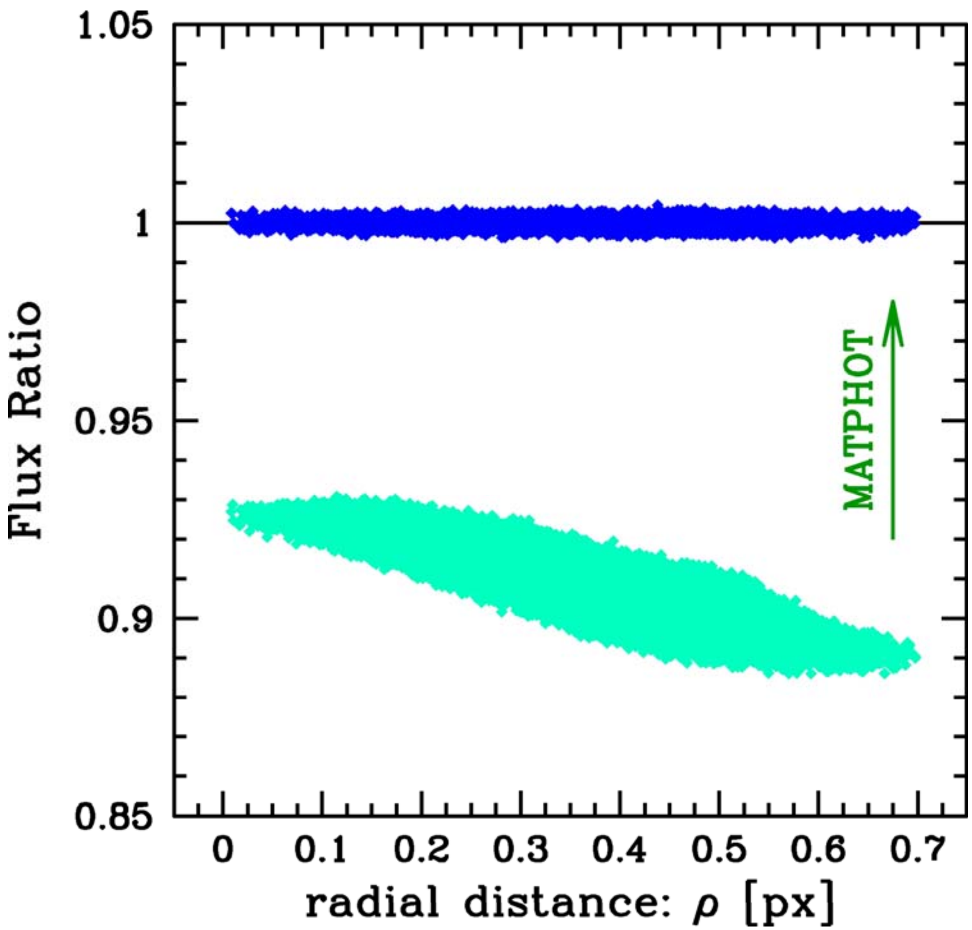

◀ random errors

◀ ***systematic*** errors

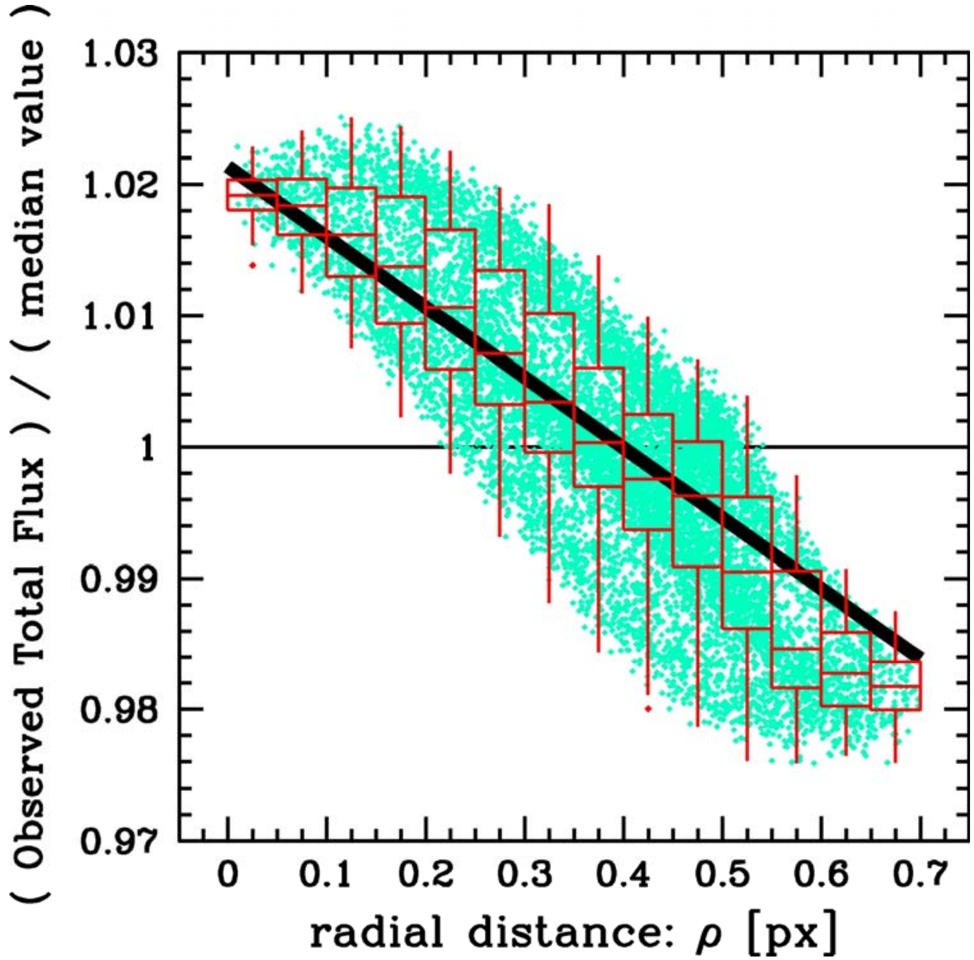

The recommended radial correction leaves a significant systematic error of a few percent.

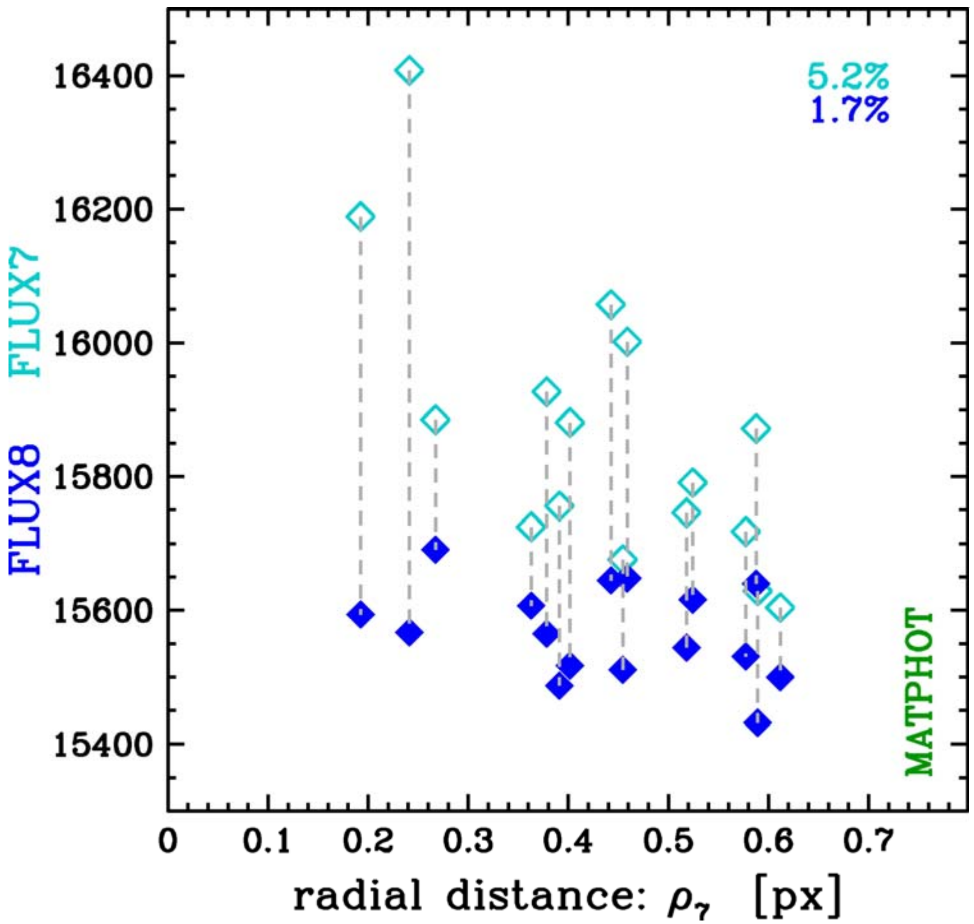

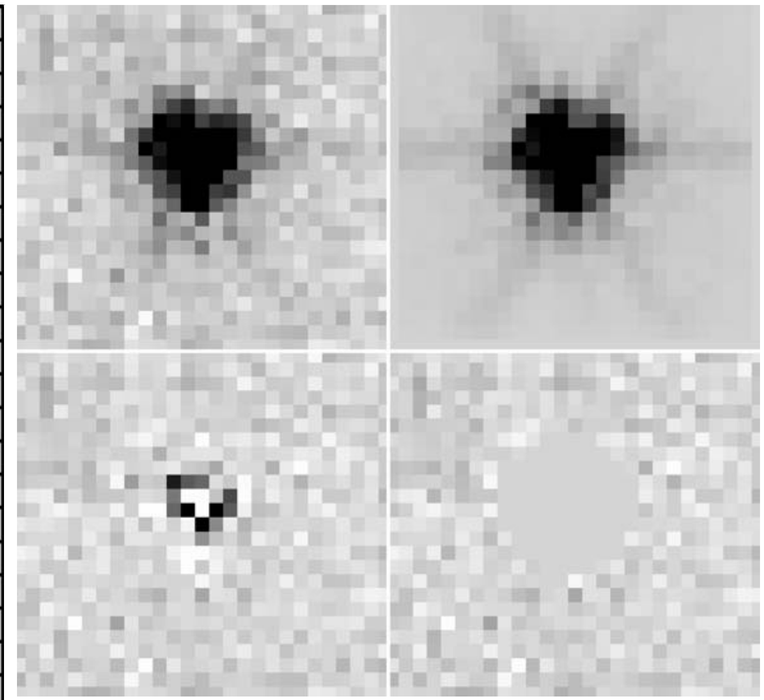

MATPHOT with residuals

A 1.7% peak-to-peak range using MATPHOT flux measurements *with residuals within 5 pixels*.

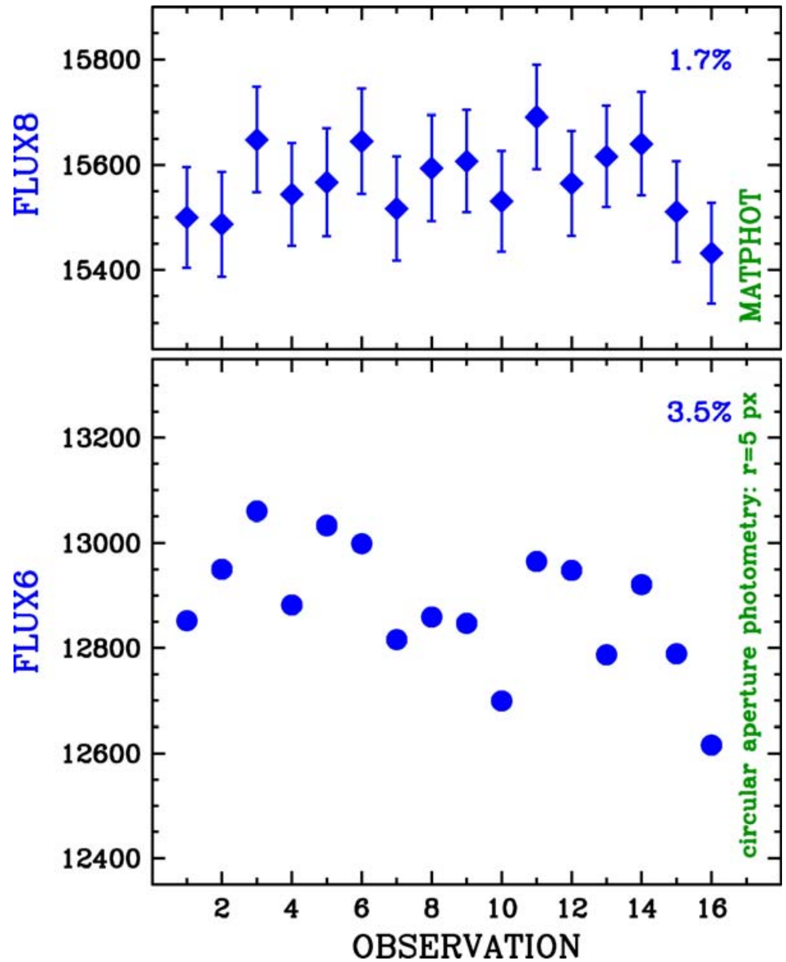

An improvement of a factor of 2 over the best results from aperture photometry using MATPHOT with residuals.

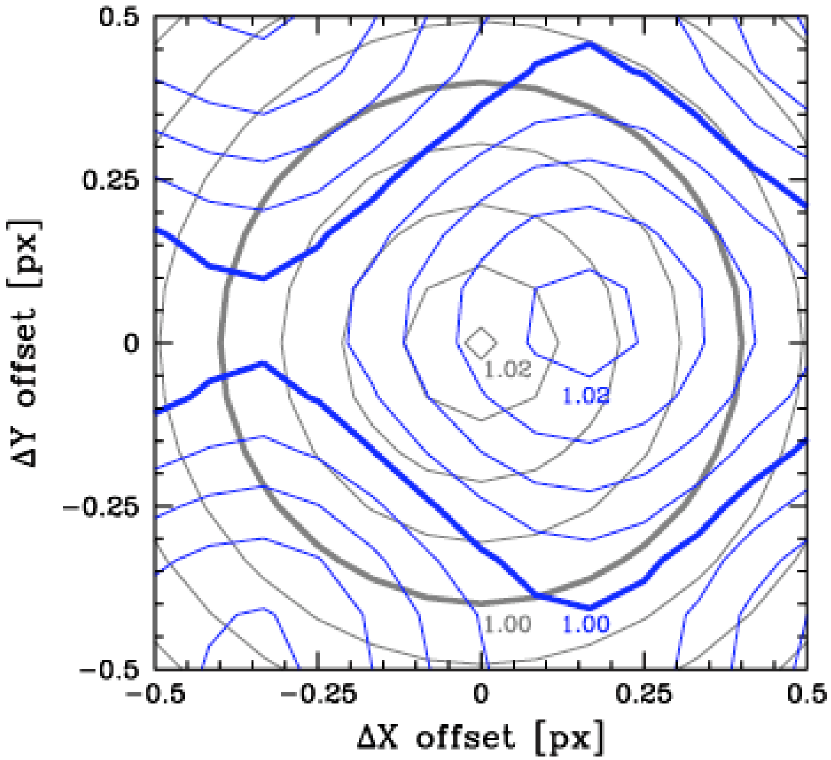

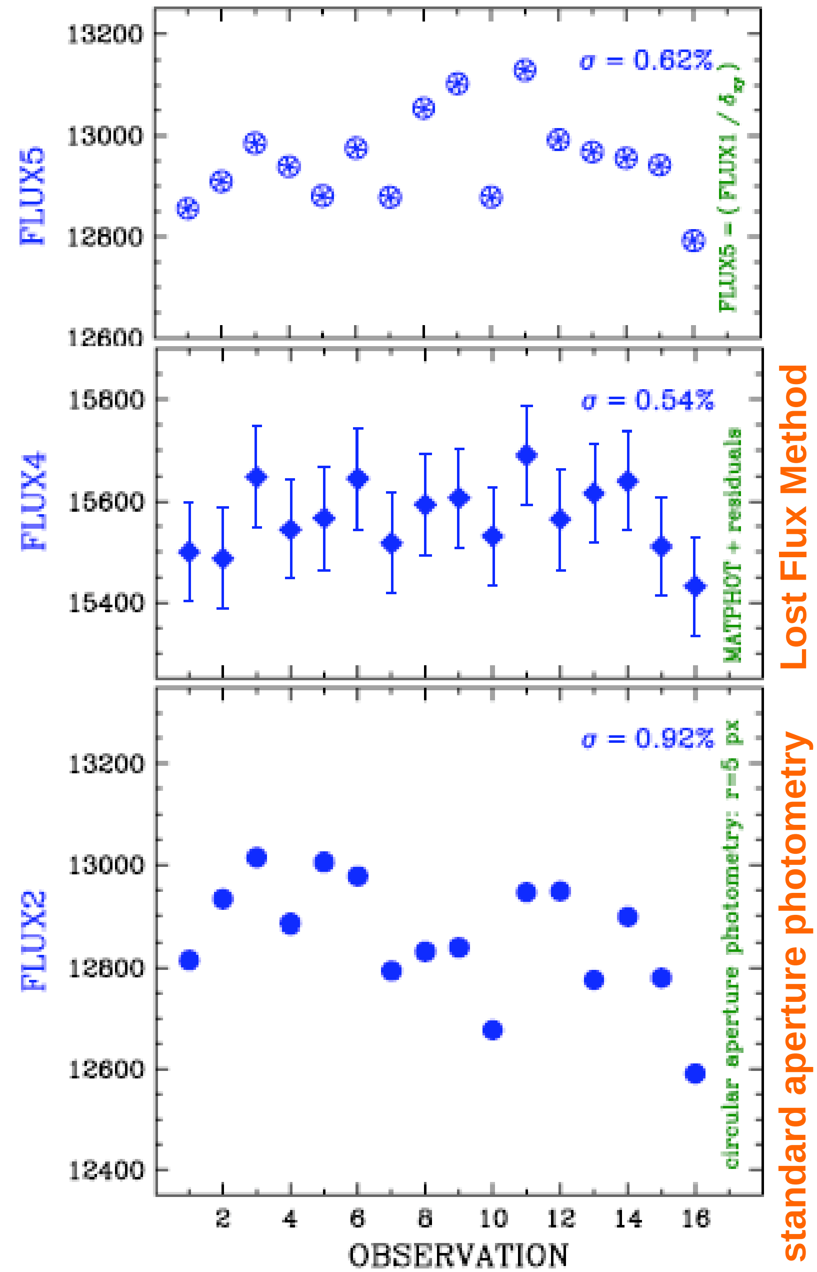

With the new 2-dimensional pixel-phase aperture-flux correction shown above, one can now achieve photometric precision with aperture photometry on bright isolated stars that is comparable to the best results produced by PSF-fitting procedures.

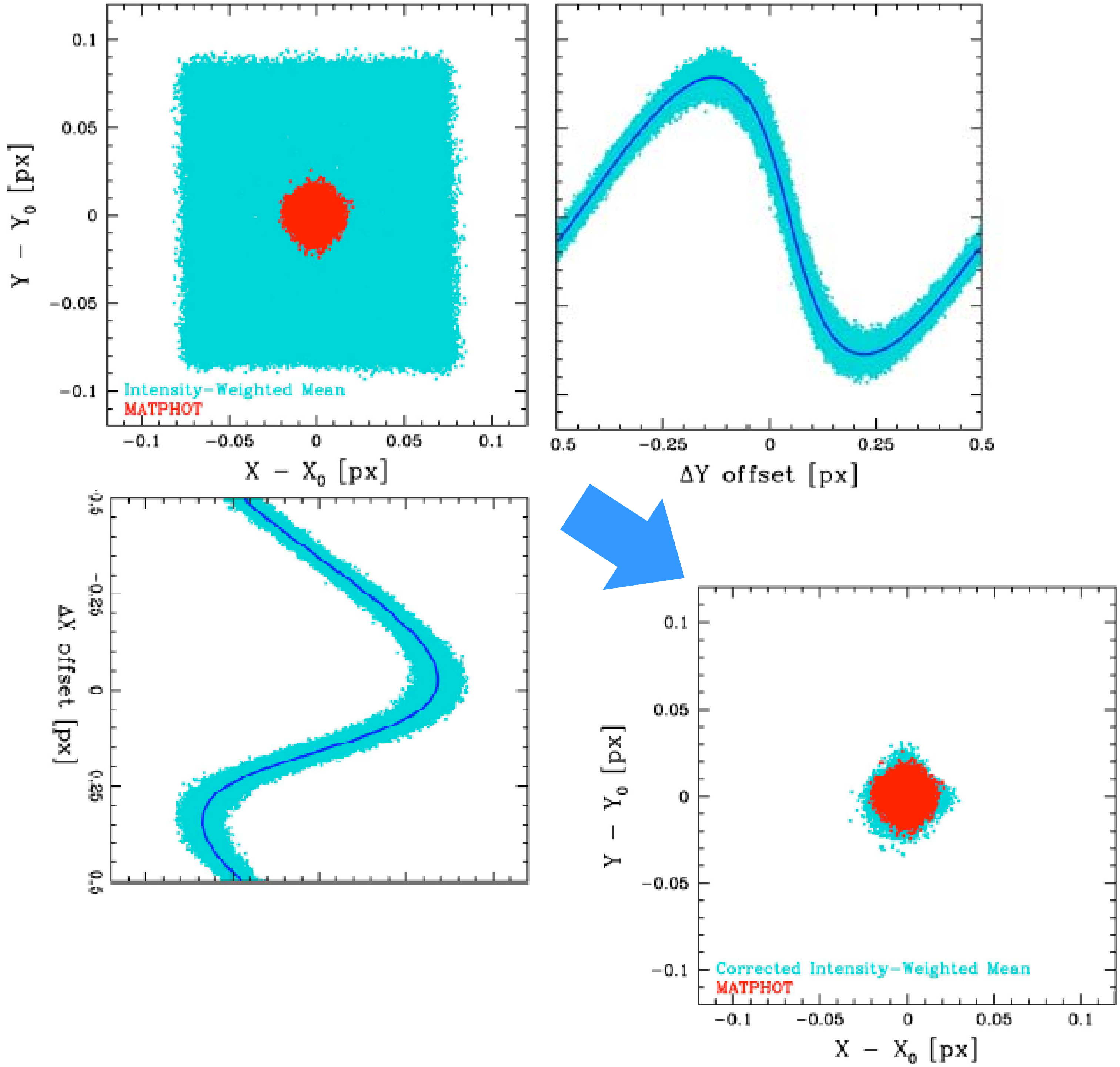

Intensity−Weighted Mean
MATPHOT
Y − Y0 [px]
X − X0 [px]
ΔY offset [px]
ΔX offset [px]
Corrected Intensity−Weighted Mean
MATPHOT
Y − Y0 [px]
X − X0 [px]

A Systematic Centroid Error

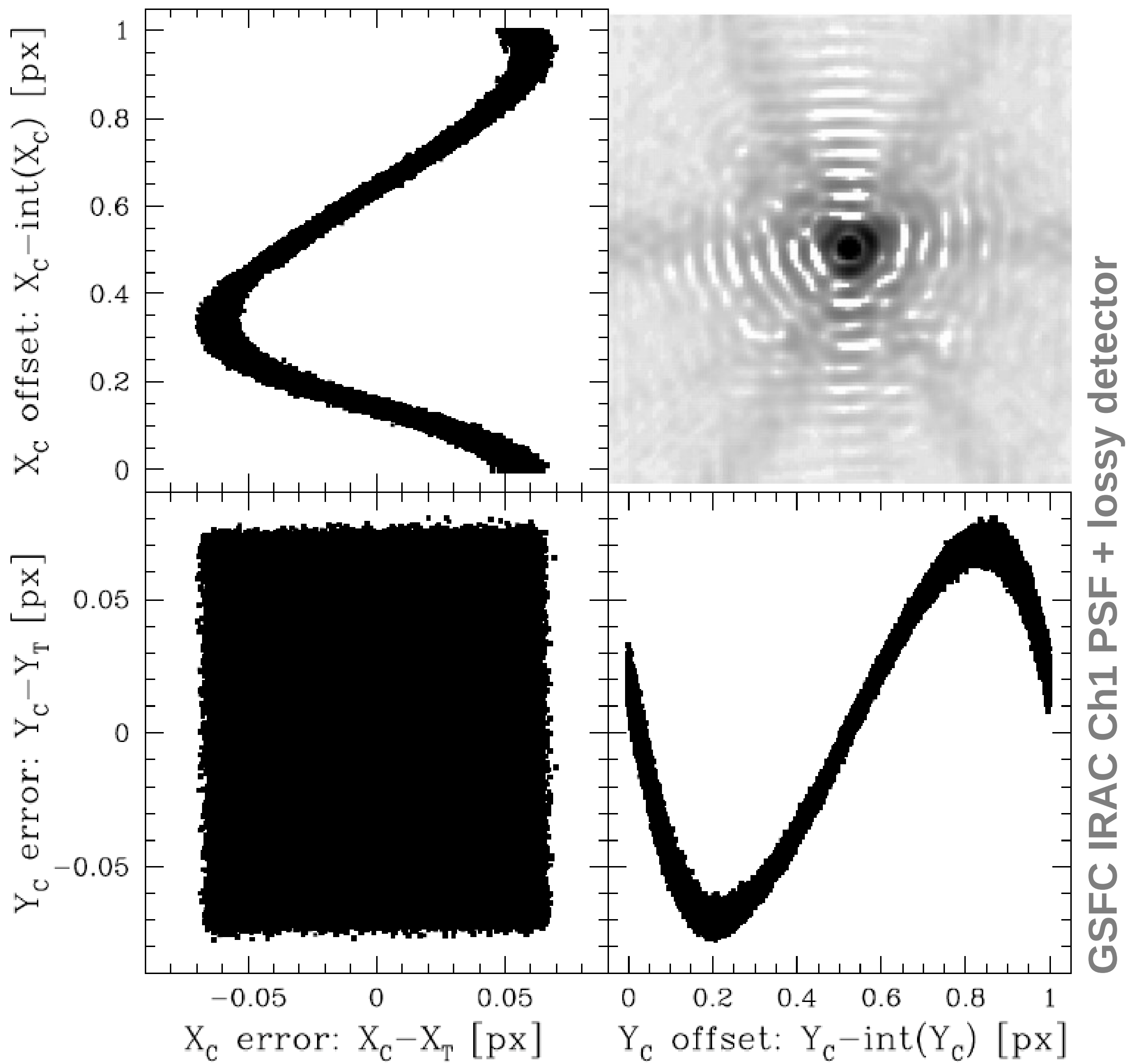

X_C offset: $X_C - \mathrm{int}(X_C)$ [px]
Y_C error: $Y_C - Y_T$ [px]
X_C error: $X_C - X_T$ [px]
Y_C offset: $Y_C - \mathrm{int}(Y_C)$ [px]
GSFC IRAC Ch1 PSF + lossy detector

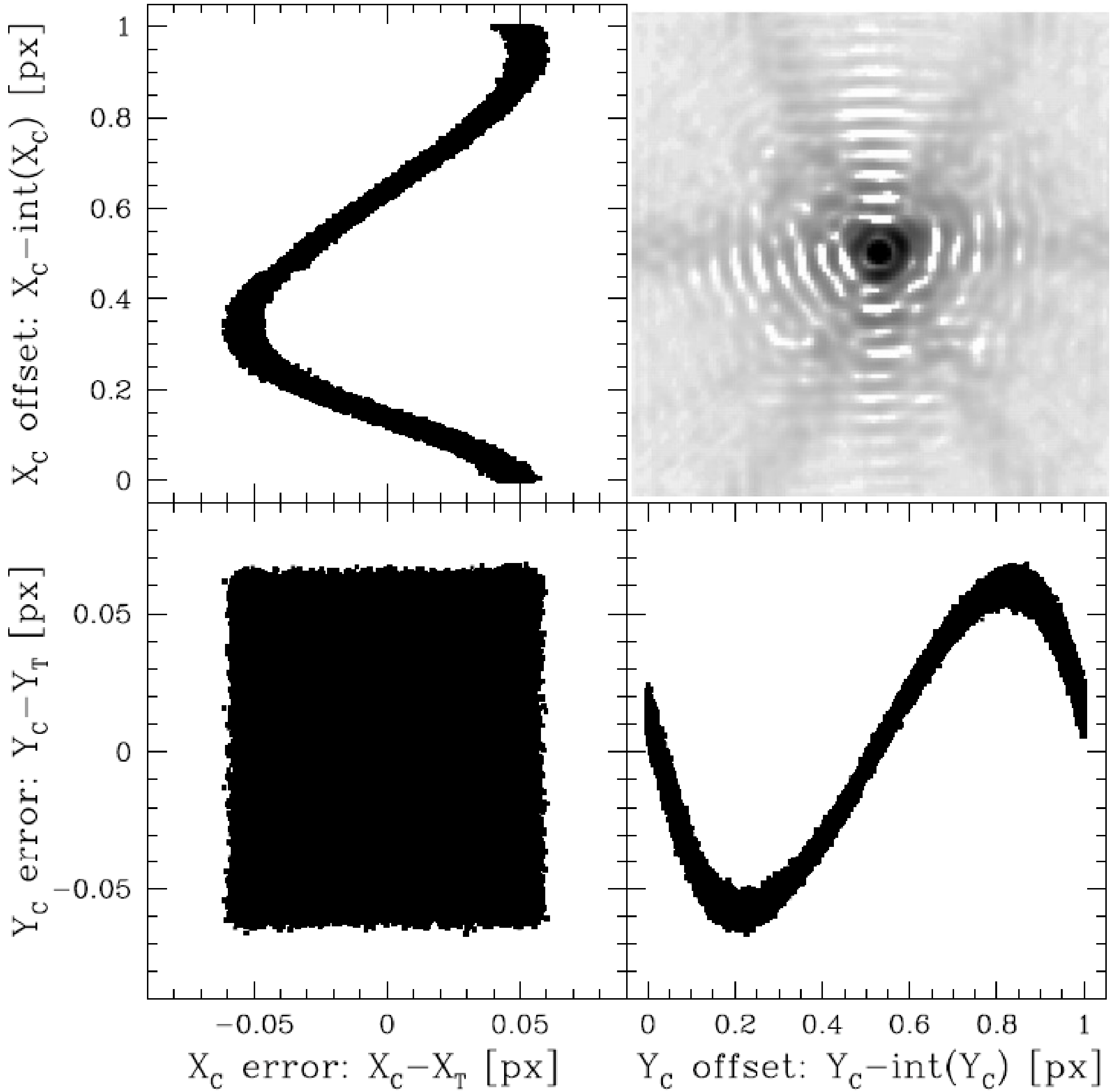

GSFC IRAC Ch1 PSF + perfect detector

TinyTim/Spitzer IRAC Ch1 PSF + perfect detector

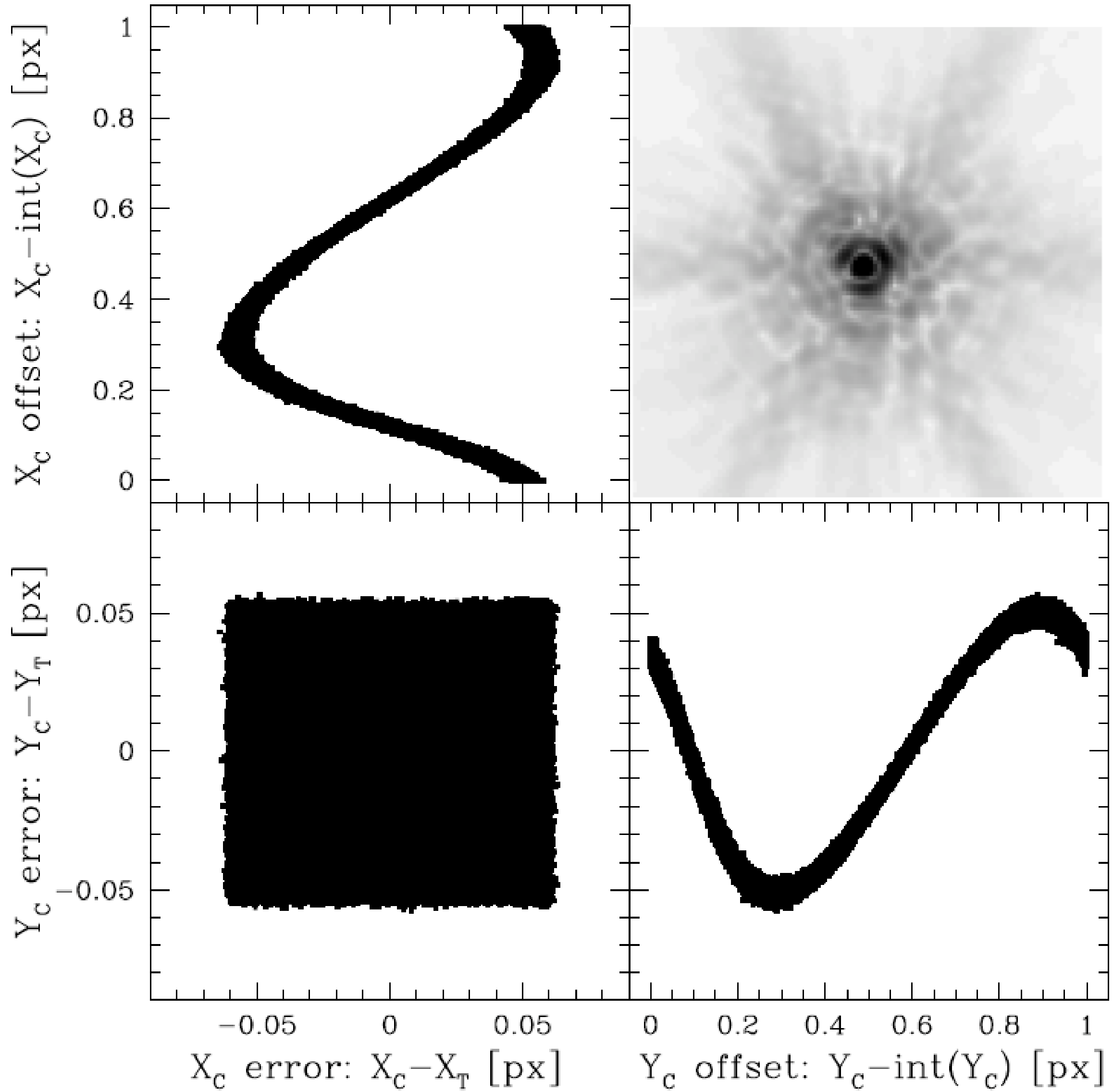

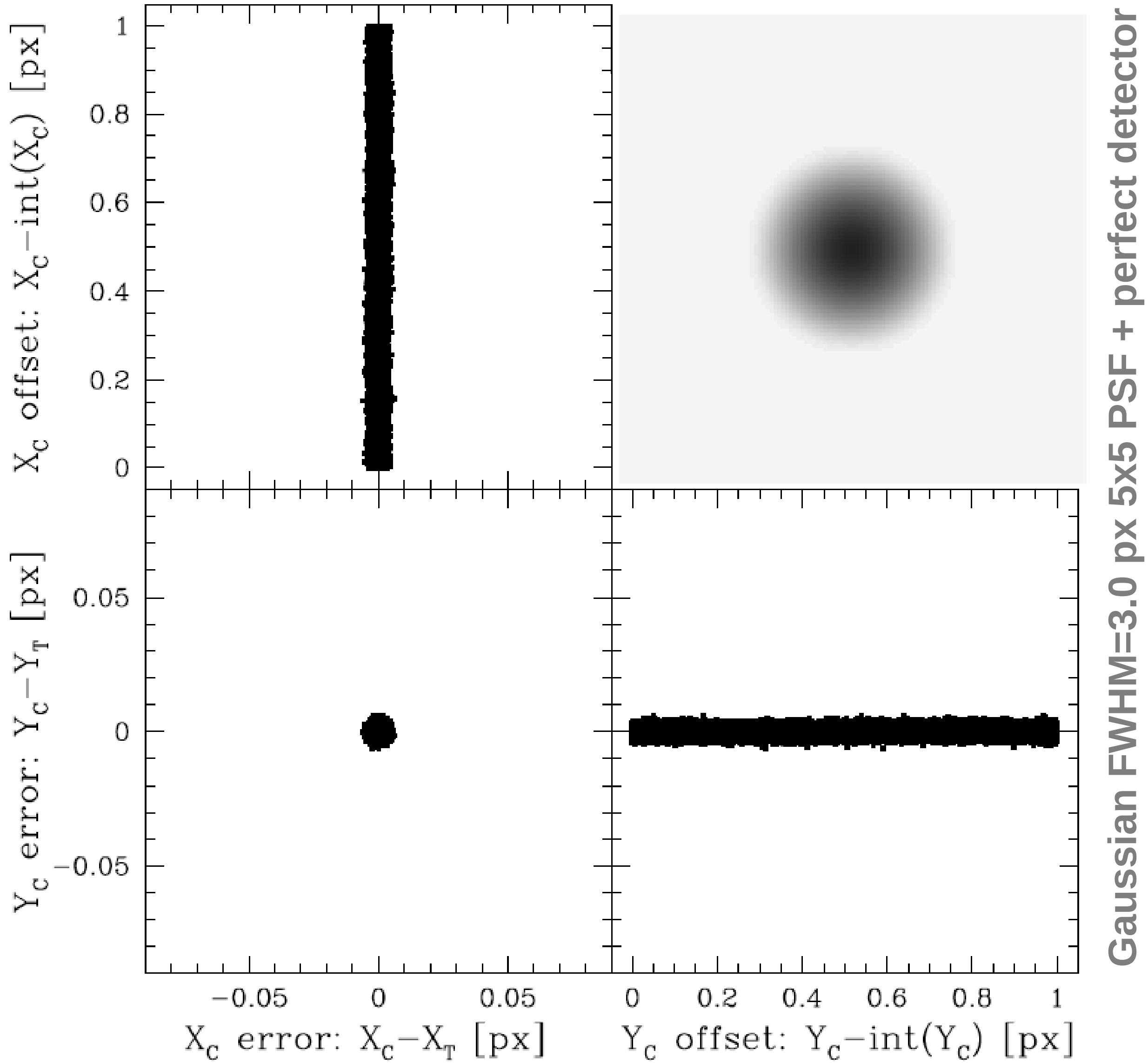

Gaussian FWHM=3.0 px 5x5 PSF + perfect detector
X_C offset: X_C−int(X_C) [px]
X_C error: X_C−X_T [px]
Y_C error: Y_C−Y_T [px]
Y_C offset: Y_C−int(Y_C) [px]
0
0.2
0.4
0.6
0.8
1
−0.05
0.05

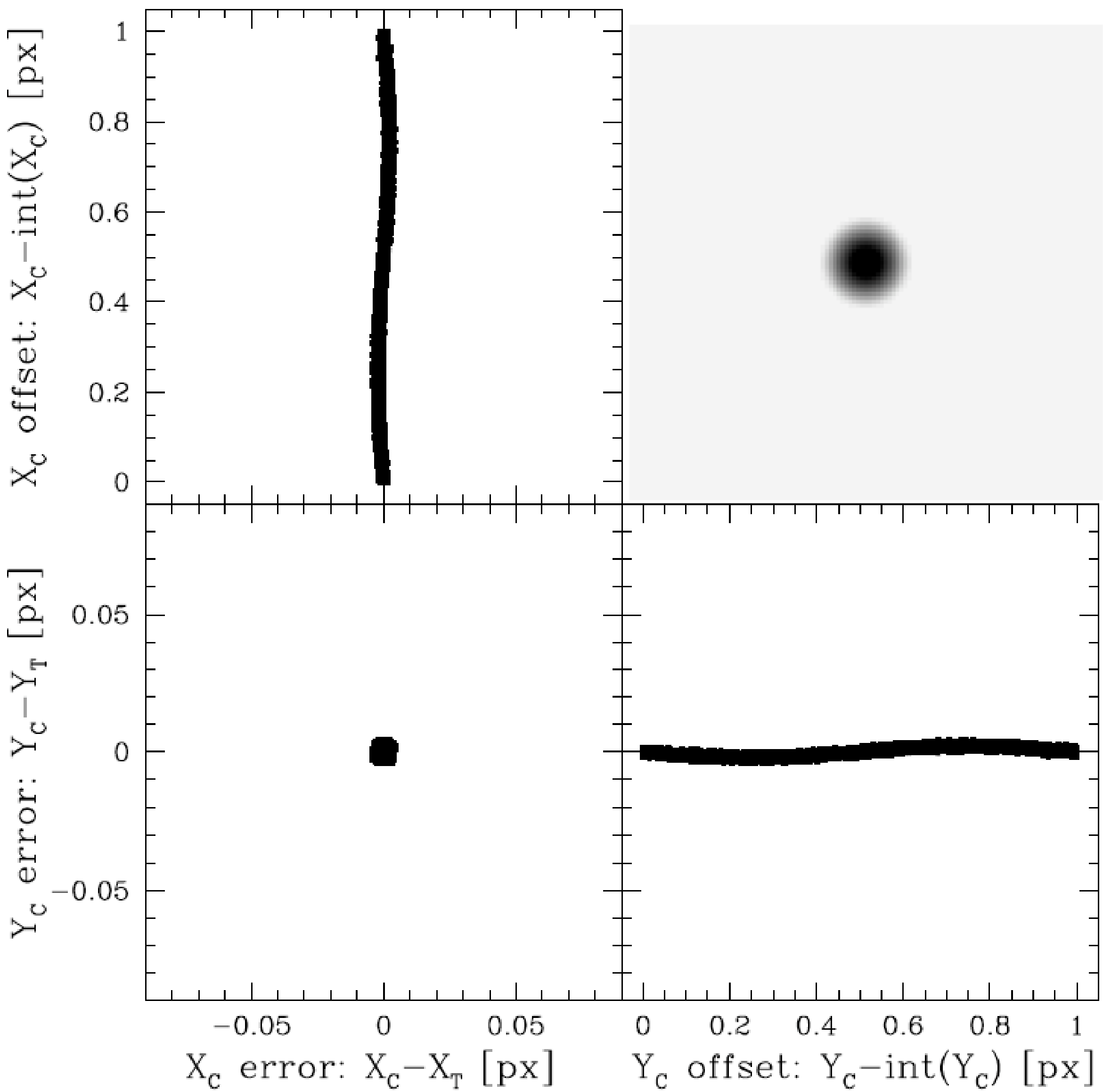

Gaussian FWHM=1.182 px 5x5 PSF + perfect detector

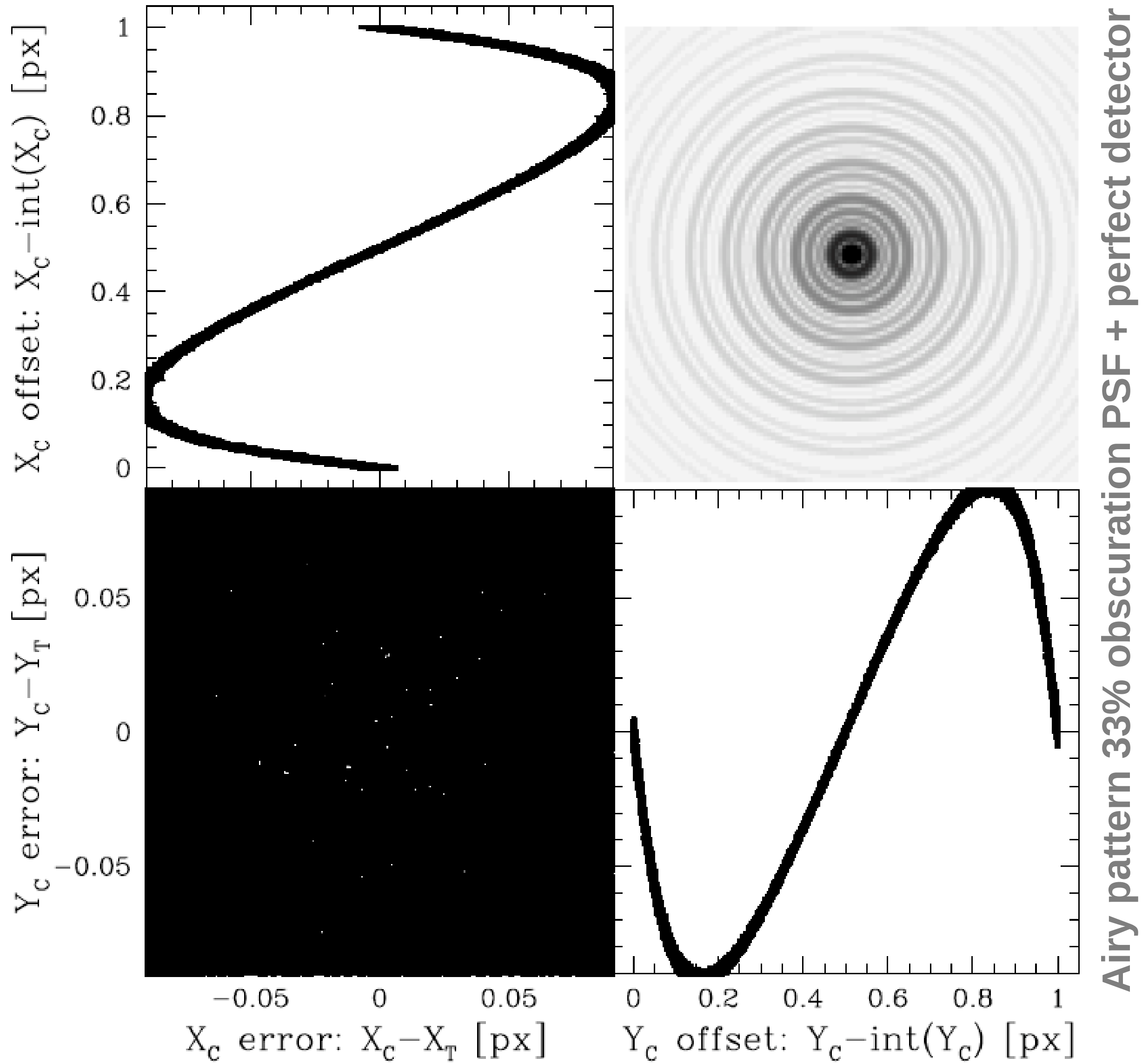

Airy pattern 33% obscuration PSF + perfect detector
X_C offset: $X_C-\mathrm{int}(X_C)$ [px]
Y_C error: Y_C-Y_T [px]
X_C error: X_C-X_T [px]
Y_C offset: $Y_C-\mathrm{int}(Y_C)$ [px]

Airy pattern 60% obscuration PSF + perfect detector

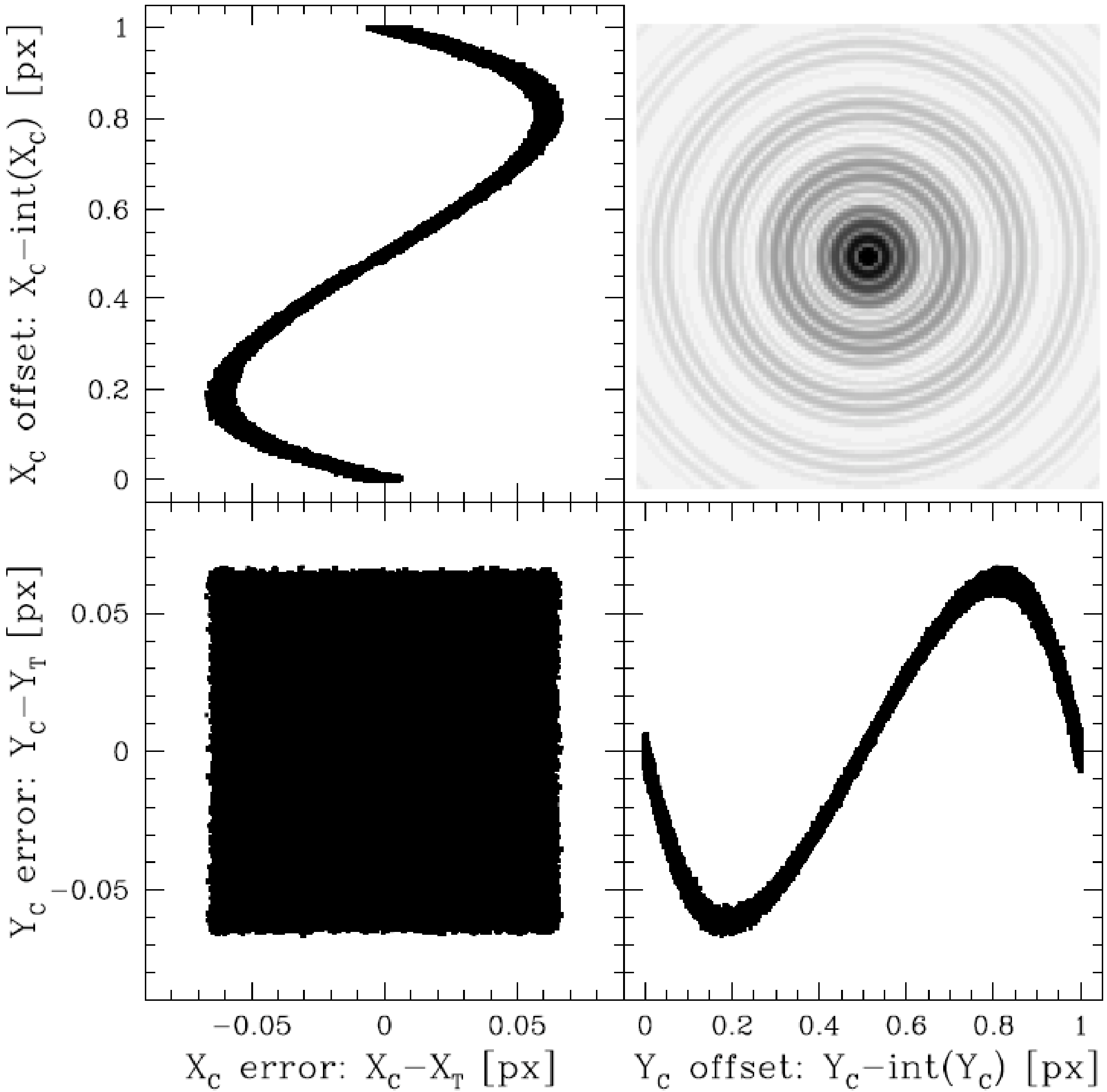

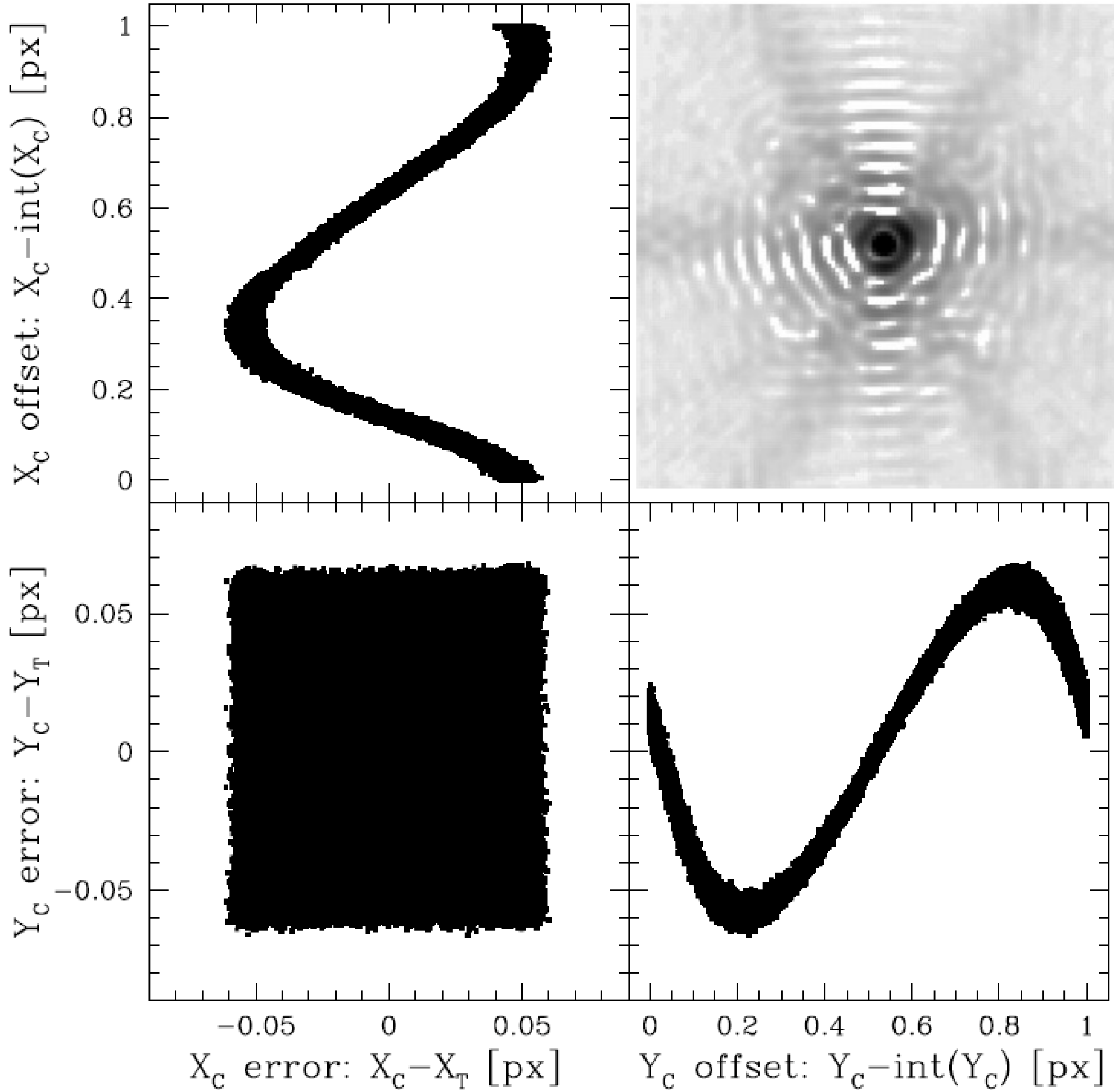

GSFC IRAC Ch1 PSF + perfect detector

❑ This systematic centroid error will be seen in space-based cameras with nearly-diffraction limited optics and undersampled focal planes.

❑ We see this effect in *Spitzer's* IRAC Ch1 camera and expect to see it in *Hubble's* NICMOS, WFPC2, and WFC3/IR instruments – as well as *James Webb Space Telescope's* NIRCam instrument.

❑ Correcting for this systematic centroid error should produce better near-field position measurements and sharper mosaics through better stacking of dithered images.

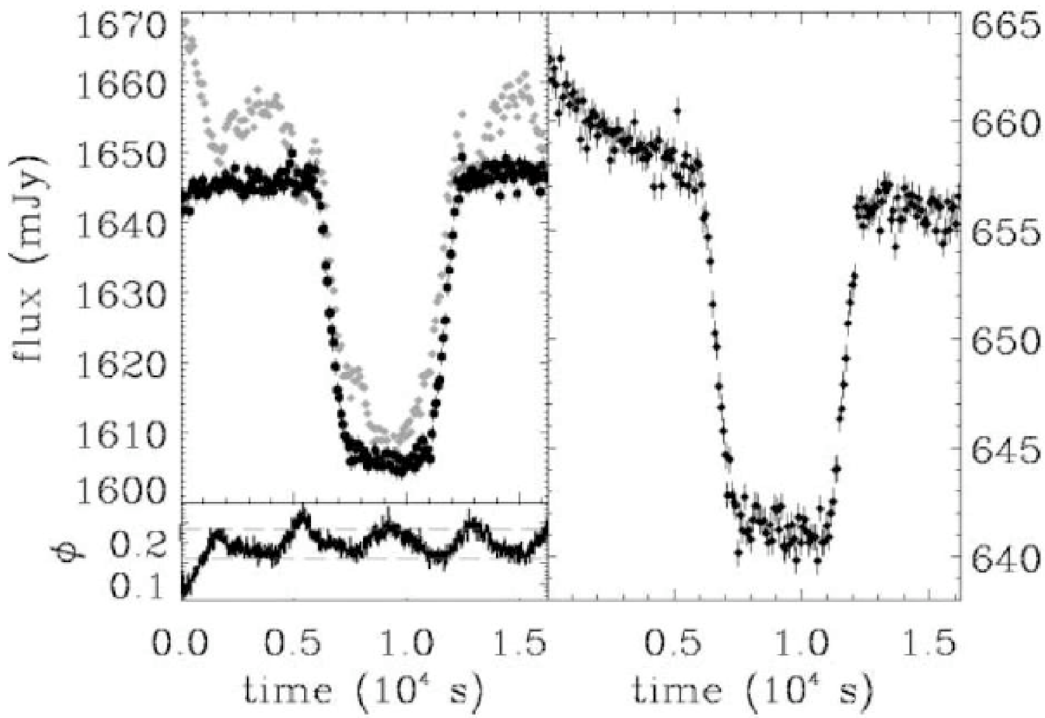

FIG. 1.—Weighted light curves in channel 1 at 3.6 μm (*left*) and channel 3 at 5.8 μm (*right*). Data are rebinned by 10. The raw light curve at 3.6 μm (*gray diamonds*) has to be corrected for large fluctuations correlated to the "pixel phase," plotted in the lower left panel. Those exposures with extreme pixel phases (beyond the dashed lines) are rejected. The corrected light curve is overplotted as black circles in the upper panel.

Figure 8: Figure 1 of Ehrenreich et al.'s article "A *SPITZER* Search for Water in the Transiting Exoplanet HD 189733b". Note the problems they had with large residuals due to "pixel-phase" correction errors.

Porting CRBLASTER to the Maestro Processor

CRBLASTER

CRBLASTER is an AISRP-funded parallel-processing application for cosmic-ray rejection in space-based CCD observations.

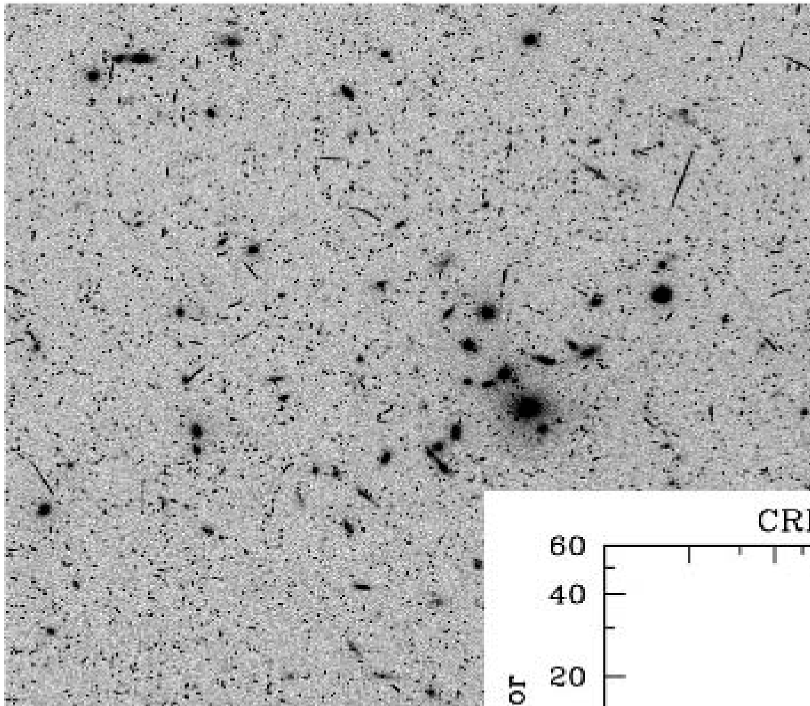

before*

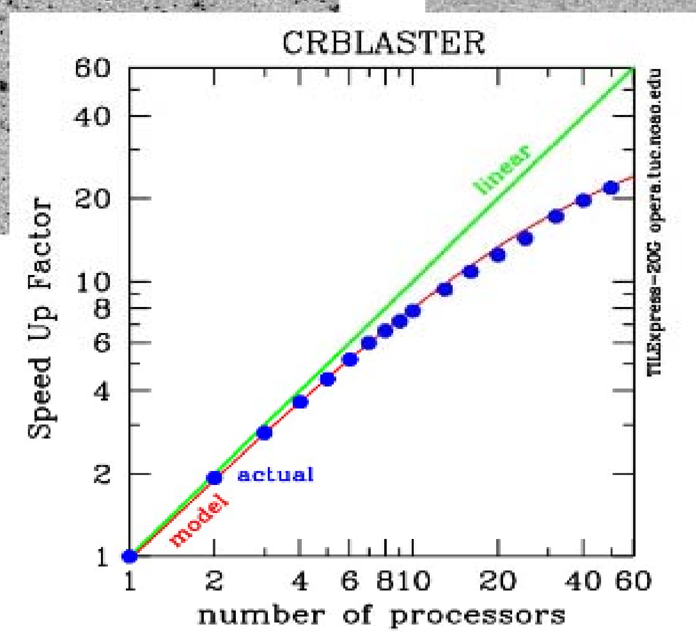

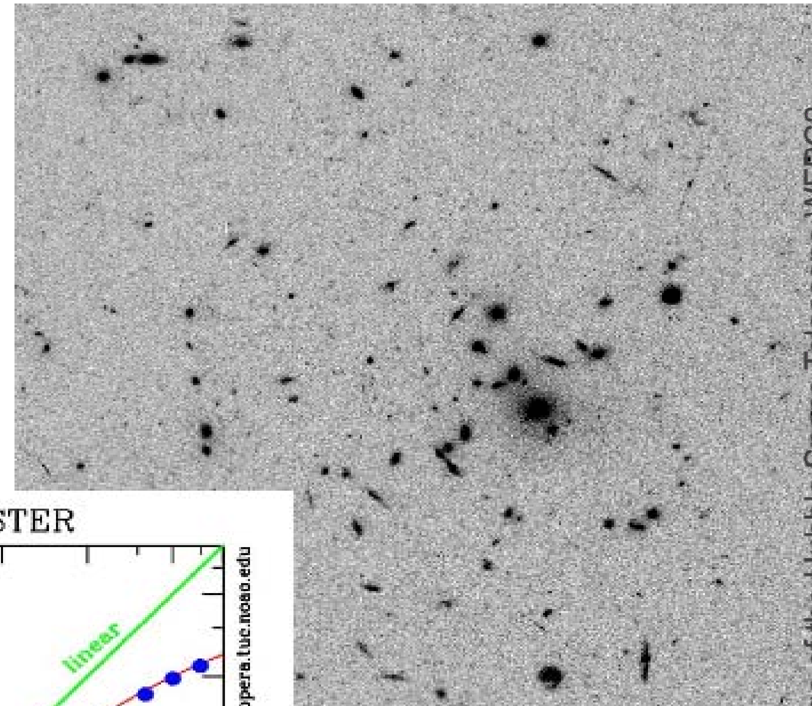

after

* The WF3 image of the Hubble Space Telescope WFPC2 observation U3060302M.C0H of the galaxy cluster MS 1137+67.

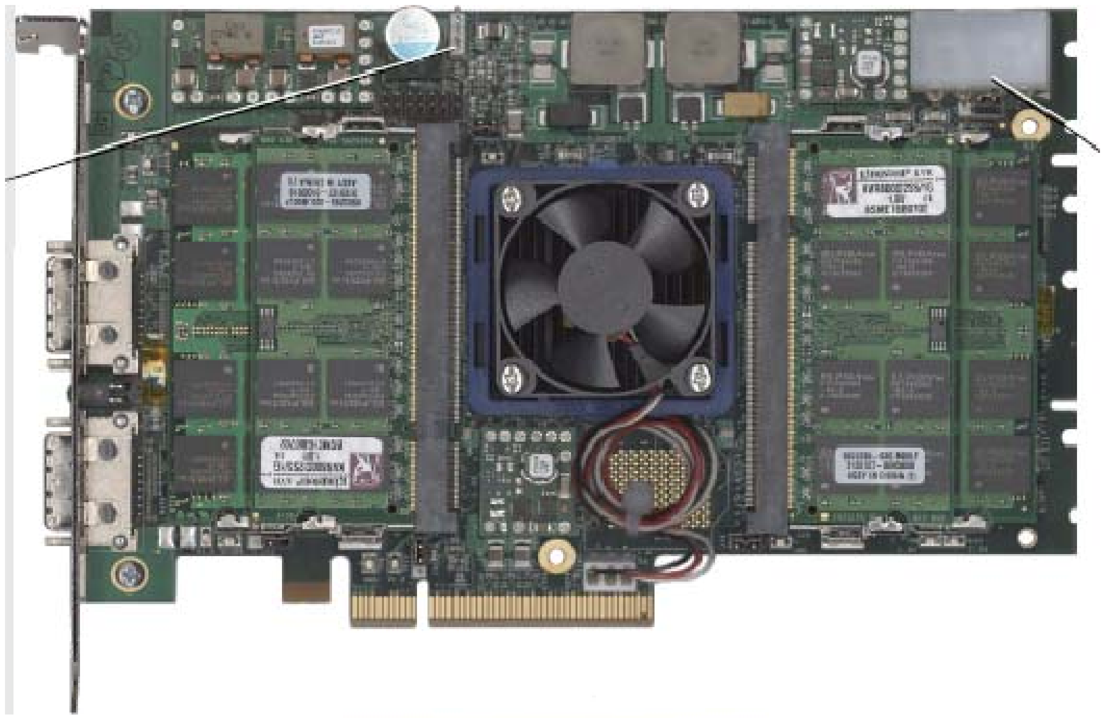

TILExpress-20G Card

TILERA
EMBEDDING MULTICORE

64 cores

in a 8x8 mesh architecture

CRBLASTER

Porting the CRBLASTER cosmic-ray rejection application to the Maestro processor.

The NASA-funded CRBLASTER cosmic-ray rejection application for space-based CCD images (e.g., Hubble Space Telescope WFPC2 instrument observations) will be ported to the low-power RHDB 49-core Maestro processor using a Tilera 64-core Tile64 platform (TILExpress-20G card) as an intermediary step.

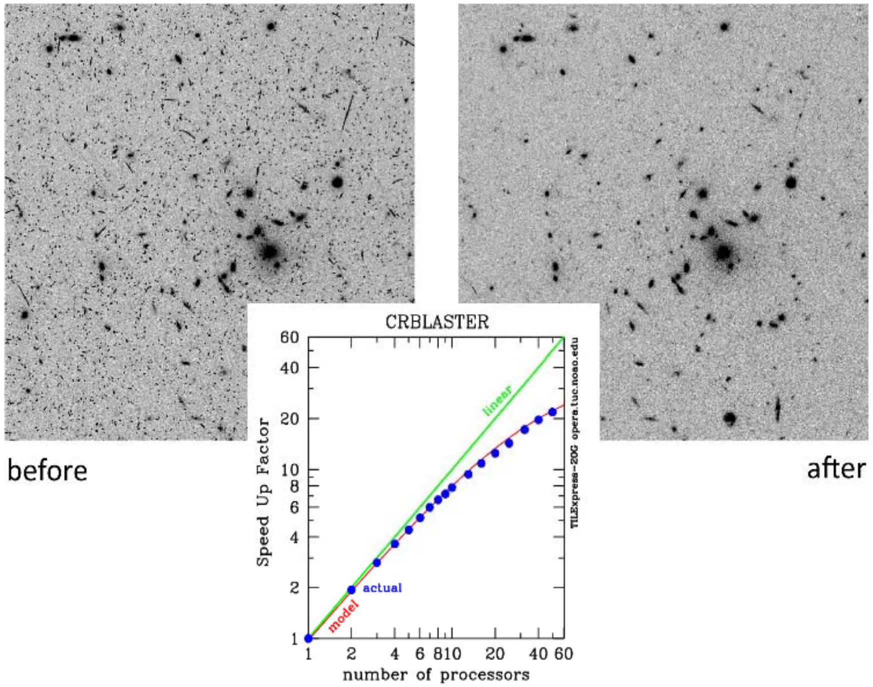

PROJECT MILESTONES

- Install TILExpress-20G card in Dell 5400 PC 09/15/2009 ✔
- Port CRBLASTER to the Tile64 platform 09/27/2009 ✔
- Run CRBLASTER on the Tile64 simulator 09/29/2009 ✔
- Port CRBLASTER to the Maestro simulator 10/04/2009 ✔
- Run CRBLASTER on a Maestro platform 2010Q2
- Contribute to TRL-6 Validation Demonstration 2010Q4

The total time spent on porting CRBLASTER to the Maestro simulator was only 24 hours by the Principal Investigator. This is remarkably quick time considering the novel nature of the Tile64/Maestro computer architecture.

- CRBLASTER has been ported to the Maestro simulator with a total work effort of only 24 hours spread over several days.
- A new image-partitioning algorithm is being developed which should raise the efficiency with 47 cores from 57% to 89%.
- Orbital debris looks like a cosmic-ray streak in a stare-mode observation. The CRBLASTER software could be modified to become a **fast real-time onboard detector of orbital debris** on a Space Based Space Surveillance (SBSS) platform using a Maestro onboard processor.

This work is supported by a grant, Interagency Order No. NNG06EC81I, from the **Applied Information Systems Research (AISR)** Program of the Science Mission Directorate of the National Aeronautics and Space Administration (NASA).